

Infrared spectra and fragmentation dynamics of isotopologue-selective mixed-ligand complexes

Peter D. Watson,¹ Gabriele Meizyte,¹ Philip A. J. Pearcy,¹ Edward I. Brewer,¹ Alice E. Green,¹ Christopher Robertson,² Martin J. Paterson,² and Stuart R. Mackenzie^{1}*

¹ Department of Chemistry, University of Oxford, Physical and Theoretical Chemistry Laboratory, South Parks Road, Oxford, United Kingdom, OX1 3QZ

² School of Engineering & Physical Sciences, Heriot-Watt University, Edinburgh, Scotland, EH14 4AS

Supporting Information

Contents:

Table S1: Cartesian coordinates of $\text{Au}(\text{CO})_n(\text{N}_2\text{O})_m^+$ complexes.....	3
Table S2: Calculated Frequencies for isotopically substituted $\text{Au}(^{13/12}\text{CO})_2(\text{N}_2\text{O})^+$ complexes.	4
Table S3: Calculated Frequencies for isotopically substituted $\text{Au}(^{13/12}\text{CO})_3(\text{N}_2\text{O})^+$ complexes.	5
Table S4 Calculated Frequencies for isotopically substituted $\text{Au}(^{13/12}\text{CO})_3(\text{N}_2\text{O})_2^+$ complexes.	7
Table S5: Relative total fragmentation yields for isotopically substituted $\text{Au}(^{12/13}\text{CO})_3(\text{N}_2\text{O})_m^+$ ($m = 1, 2$) complexes.	8
Figure S1: Representative portion of the $\text{Au}(^{13}\text{CO})_n(\text{N}_2\text{O})_m^+$ mass spectrum.....	9
Figure S2: Representative mass spectra showing the isotopologue distribution with increasing ^{13}CO concentration	10
Figure S3: Representative mass spectra of the $\text{Au}(^{13/12}\text{CO})_3(\text{N}_2\text{O})^+$ illustrating photofragmentation.....	11
Figure S4: Representative mass spectra of the $\text{Au}(^{13/12}\text{CO})_3(\text{N}_2\text{O})_2^+$ illustrating photofragmentation	12
Figure S5: Comparison of experimental and simulated infrared action spectra of $\text{Au}(^{13/12}\text{CO})_2(\text{N}_2\text{O})^+$ complexes....	13
Figure S6: Comparison of experimental and simulated infrared action spectra of $\text{Au}(^{13/12}\text{CO})_3(\text{N}_2\text{O})^+$ complexes....	14
Figure S7: Comparison of experimental and simulated infrared action spectra of $\text{Au}(^{13/12}\text{CO})_3(\text{N}_2\text{O})_2^+$ complexes...	15
Figure S8: Potential energy surface cuts.....	16

Table S1: Cartesian coordinates of $\text{Au}(\text{CO})_n(\text{N}_2\text{O})_m^+$ complexes in both low symmetry (C_1) and enforced higher symmetry (C_{2v} , C_{3v} and D_{3h}).

C2N1	C_1			C_{2v}		
Au	-0.692469	0.038511	0.000005	0.000000	0.000000	0.692605
C	-0.570813	2.020114	-0.000123	0.000000	1.981950	0.779194
O	-0.507316	3.132274	0.000063	0.000000	3.094626	0.833871
C	-0.983585	-1.922371	-0.000123	0.000000	-1.981950	0.779194
O	-1.155117	-3.023144	0.000063	0.000000	-3.094626	0.833871
O	4.608706	-0.301456	-0.000015	0.000000	0.000000	-4.616481
N	3.449621	-0.198871	0.000006	0.000000	0.000000	-2.329437
N	2.330563	-0.099730	0.000022	0.000000	0.000000	-3.452875

C3N1	C_1			C_{3v}		
Au	-0.617366	-0.001192	-0.001168	0.000000	0.000000	0.617473
C	-0.671275	-1.945370	0.683188	0.000000	2.061283	0.675590
O	-0.707644	-2.998729	1.053692	0.000000	3.177813	0.714163
C	-0.666742	0.377717	-2.027731	-1.785124	-1.030642	0.675590
O	-0.700441	0.582798	-3.125426	-2.752067	-1.588907	0.714163
C	-0.688270	1.564487	1.338901	1.785124	-1.030642	0.675590
O	-0.734068	2.412482	2.064787	2.752067	-1.588907	0.714163
O	4.646397	0.008400	0.010753	0.000000	0.000000	-4.647038
N	3.482630	0.006282	0.008119	0.000000	0.000000	-2.360108
N	2.359613	0.004231	0.005547	0.000000	0.000000	-3.483412

C3N2	C_1			D_{3h}		
Au	-0.000315	0.001423	-0.001546	0.000000	0.000000	0.000000
C	-0.004118	0.764599	-1.913965	0.000000	2.059158	0.000000
O	-0.006088	1.179199	-2.951874	0.000000	3.176813	0.000000
C	0.001025	-2.036463	0.293939	1.783283	-1.029579	0.000000
O	0.002515	-3.142604	0.453927	2.751201	-1.588407	0.000000
C	0.003327	1.276368	1.615503	-1.783283	-1.029579	0.000000
O	0.005714	1.968440	2.493094	-2.751201	-1.588407	0.000000
O	5.416425	-0.004376	0.005337	0.000000	0.000000	5.416255
N	4.251328	-0.004078	0.001995	0.000000	0.000000	3.128067
N	3.128244	-0.003903	-0.001307	0.000000	0.000000	4.251156
O	-5.416135	-0.006810	0.006568	0.000000	0.000000	-5.416255
N	-4.251040	-0.003884	0.006394	0.000000	0.000000	-3.128067
N	-3.127951	-0.001027	0.006184	0.000000	0.000000	-4.251156

Table S2: Calculated Frequencies for isotopically substituted Au(^{13/12}CO)₂(N₂O)⁺ complexes. Frequencies are ordering by descending symmetry label where appropriate and nominal descriptive assignments of the modes are provided. Modes associated with N₂O are scaled with respect to the N=N stretch in free N₂O stretch (2223.5cm⁻¹, SF = 0.9322) and CO modes are scaled to experiment (SF = 0.9674).

Alt Symm	Freq.	Assignment	Symm	¹² C ² N ¹	Scaled	¹² C ¹ ¹³ C ¹ N ¹	Scaled	¹³ C ² N ¹	Scaled
7a₁	2397	N ₂ O asymm. stretch	<i>a</i>	2397	2234	2397	2254	2397	2234
6a₁	2344	CO symm. stretch	<i>a</i>	2344	2267	2330	2234	2289	2214
5a₁	1403	N ₂ O symm. stretch	<i>a</i>	1403	1308	1403	1308	1403	1308
4a₁	406	OCAu symm. in-plane bend	<i>a</i>	406	393	401	388	396	383
3a₁	399	CAuC symm. stretch	<i>a</i>	399	386	395	382	390	377
2a₁	64	Au-N ₂ O stretch	<i>a</i>	64	62	64	62	64	62
1a₁	48	Au-N ₂ O stretch	<i>a</i>	48	45	48	46	48	45
1a₂	310	OCAu out-plane out-phase bend	<i>a</i>	311	300	305	296	301	291
4b₁	641	ONN out-plane bend	<i>a</i>	641	597	641	597	641	597
3b₁	403	OCAu symm. out-plane bend	<i>a</i>	403	390	397	384	390	377
2b₁	62	CAuC out-plane bend	<i>a</i>	62	62	62	62	62	62
1b₁	48	N ₂ O inter. out-plane rotation	<i>a</i>	48	46	48	45	48	46
6b₂	2306	CO asymm. stretch	<i>a</i>	2306	2231	2266	2192	2253	2180
5b₂	642	ONN in-plane bend	<i>a</i>	642	598	642	598	642	598
4b₂	357	CAuC asymm. stretch	<i>a</i>	357	345	354	342	352	341
3b₂	314	OCAu in-plane out-phase bend	<i>a</i>	315	304	310	299	305	295
2b₂	39	N ₂ O inter. in-plane rotation	<i>a</i>	39	37	39	37	39	37
1b₂	2i	N ₂ O inter. bend	<i>a</i>	1	1	1	1	1	1
				<i>zpe</i> (eV)	0.755 0.720	0.750 0.715	0.715	0.745	0.710
						<i>Δzpe</i> (eV)		0.005	0.010

Table S3: Calculated Frequencies for isotopically substituted $\text{Au}^{(13/12)}\text{CO}_3(\text{N}_2\text{O})^+$ complexes. Frequencies are ordering by descending symmetry label where appropriate and nominal descriptive assignments of the modes are provided. Modes associated with N_2O are scaled with respect to the $\text{N}=\text{N}$ stretch in free N_2O stretch (2223.5cm^{-1} , $\text{SF} = 0.9322$) and CO modes are scaled to experiment ($\text{SF} = 0.9674$).

Alt	Freq.	Assignment	Symm	¹² C3N1	Scaled	¹² C2 ¹³ C1N1	Scaled	¹² C1 ¹³ C2N1	Scaled	¹³ C3N1	Scaled
7a₁	2399	N ₂ O asymm. stretch	<i>a</i>	2400	2237	2399	2236	2399	2236	2398	2236
6a₁	2300	(CO) ₃ symm. stretch	<i>a</i>	2299	2224	2293	2219	2286	2211	2247	2173
5a₁	1403	N ₂ O symm. stretch	<i>a</i>	1403	1308	1403	1308	1403	1308	1403	1308
4a₁	354	(CO) ₃ out-of-plane bend	<i>a</i>	354	342	350	339	346	335	342	331
3a₁	323	(CO)3 symm. inter. stretch	<i>a</i>	324	313	322	311	320	309	318	308
2a₁	62	N ₂ O inter. stretch, Au-C-O inter. bend	<i>a</i>	62	60	62	60	62	60	62	60
1a₁	53	N ₂ O inter. stretch, Au-CO inter. bend	<i>a</i>	53	51	53	51	53	51	53	51
1a₂	256	(CO)3 symm. inter. bend	<i>a</i>	256	248	254	245	251	243	249	240
8e	2275	(CO) ₂ asymm. stretch	<i>a</i>	2275	2201	2275	2201	2236	2163	2223	2151
8e	2275	(CO) ₂ asymm. stretch	<i>a</i>	2275	2201	2229	2156	2223	2151	2223	2151
7e	641	N ₂ O bend	<i>a</i>	640	597	641	597	641	597	641	597
7e	641	N ₂ O bend	<i>a</i>	640	597	641	597	641	597	641	597
6e	401	(CO) ₃ planar bend	<i>a</i>	401	388	400	387	396	383	390	377
6e	401	(CO)2 planar bend, CO inter. stretch	<i>a</i>	401	388	395	382	391	378	390	377
5e	244	(CO) ₃ symm. out-of-plane bend	<i>a</i>	244	236	243	235	241	233	236	229
5e	244	(CO) ₂ asymm. out-of-plane bend	<i>a</i>	243	236	239	231	236	229	236	228
4e	214	(CO) ₂ symm. inter. bend, CO inter. stretch	<i>a</i>	214	207	213	206	212	205	210	204
4e	214	(CO) ₂ symm. inter. bend, CO inter. stretch	<i>a</i>	214	207	213	206	211	205	210	203
3e	49	N ₂ O inter. bend	<i>a</i>	48	48	49	49	49	49	49	49
3e	49	N ₂ O inter. bend	<i>a</i>	48	48	49	49	49	49	49	49
2e	42	N ₂ O inter. bend	<i>a</i>	41	41	43	42	42	42	42	42
2e	42	N ₂ O inter. bend	<i>a</i>	41	41	42	42	42	42	42	42
1e	18	Au-(CO) ₂ inter. twist	<i>a</i>	18	18	18	18	18	18	18	18
1e	18	Au-(CO) ₂ inter. twist	<i>a</i>	18	18	18	18	18	18	18	18

<i>zpe</i> (eV)	0.924	0.884	0.920	0.879	0.915	0.875	0.911	0.870
			Δzpe (eV)	0.004	0.009		0.013	

Table S4 Calculated Frequencies for isotopically substituted $\text{Au}^{(13/12)}\text{CO}_3(\text{N}_2\text{O})_2^+$ complexes. Frequencies are ordering by descending symmetry label where appropriate and nominal descriptive assignments of the modes are provided. Modes associated with N_2O are scaled with respect to the $\text{N}=\text{N}$ stretch in free N_2O stretch (2223.5cm^{-1} , $\text{SF} = 0.9322$) and CO modes are scaled to experiment ($\text{SF} = 0.9674$).

Alt											
Symm	Freq.	Assignment	Symm	¹² C ¹³ N2	Scaled	¹² C ¹³ C ¹³ N2	Scaled	¹² C ¹³ C ¹³ N2	Scaled	¹³ C ¹³ N2	Scaled
5a' ₁	2396	In-phase N ₂ O asymm. stretch	a	2396	2234	2396	2234	2396	2234	2396	2234
4a' ₁	2296	In-phase CO stretch	a	2296	2221	2290	2215	2282	2208	2243	2170
3a' ₁	1398	In-phase N ₂ O symm. stretch	a	1398	1303	1398	1303	1398	1303	1398	1303
2a' ₁	325	Symm. Au-(CO) ₃ stretch	a	325	325	324	324	322	322	320	320
1a' ₁	51	Symm. N ₂ O inter. stretch	a	51	51	51	51	51	51	51	51
1a' ₂	256	Au-(CO) ₃ twist	a	256	247	253	245	251	243	248	240
7e'	2271	Out-phase CO stretch	a	2271	2197	2271	2197	2232	2160	2219	2147
7e'	2271	Out-phase CO stretch	a	2271	2197	2225	2153	2219	2147	2219	2147
6e'	640	Out-phase N ₂ O bend	a	640	597	640	597	640	597	640	597
6e'	640	Out-phase N ₂ O bend	a	640	597	640	597	640	597	640	597
5e'	403	C-Au-C scissor	a	403	390	402	388	398	385	392	379
5e'	403	C-Au-C rock	a	403	390	397	384	393	380	391	379
4e'	218	(CO) ₂ symm. inter. bend, CO inter. stretch	a	218	211	217	210	216	209	214	207
4e'	218	(CO) ₂ symm. inter. bend, CO inter. stretch	a	218	211	217	210	216	209	214	207
3e'	48	Au-(CO) ₂ bend, N ₂ O rotation	a	48	48	48	48	48	48	48	48
3e'	48	Au-(CO) ₂ bend, N ₂ O rotation	a	48	48	48	48	48	48	48	48
2e'	38	In-phase N ₂ O rotation	a	38	38	38	38	38	38	38	38
2e'	38	In-phase N ₂ O rotation	a	38	38	38	38	38	38	38	38
1e'	7	N ₂ O-Au-N ₂ O inter. bend	a	7	6	7	7	7	7	7	7
1e'	7	N ₂ O-Au-N ₂ O inter. bend	a	7	6	7	6	7	6	7	6
4a'' ₂	2393	Out-phase N ₂ O asymm. stretch	a	2393	2231	2393	2231	2393	2231	2393	2231
3a'' ₂	1397	Out-phase N ₂ O symm. stretch	a	1397	1303	1397	1303	1397	1303	1397	1303
2a'' ₂	354	Au-(CO) ₃ wag	a	354	342	350	339	346	335	342	331
1a'' ₂	56	Au-(CO) ₃ inter. wag	a	56	54	56	54	56	54	56	54
3e''	640	In-phase N ₂ O bend	a	640	597	640	597	640	597	640	597
3e''	640	In-phase N ₂ O bend	a	640	597	640	597	640	597	640	597
2e''	246	Au-(CO) ₂ twist	a	246	238	246	238	243	235	238	231
2e''	246	Au-(CO) ₂ wag	a	246	238	241	233	238	231	238	231
1e''	17	N ₂ O-Au-N ₂ O inter. tilt	a	17	16	17	16	17	16	17	16
1e''	17	N ₂ O-Au-N ₂ O inter. tilt	a	17	16	17	16	17	16	17	16

2a	43	Asymm. N ₂ O inter. stretch	<i>a</i>	43	42	43	42	43	42	43	42
1a	41	Out-of-phase N ₂ O rotation	<i>a</i>	41	39	41	39	41	39	41	39
1a	41	Out-of-phase N ₂ O rotation	<i>a</i>	41	39	41	39	41	39	41	39
<i>zpe</i> (eV)				1.246	1.184	1.242	1.180	1.237	1.175	1.232	1.171
				<i>Δzpe</i> (eV)		0.004		0.009		0.014	

Table S5: (Right) Relative total fragmentation yields for isotopically substituted Au(^{13/12}CO)₃(N₂O)_m⁺ (m = 1,2) complexes. (Left) Simplified relative total fragmentation yields ignoring isotope labelling.

Fragmentation Yield						Simplified			
C3N1									
	¹² CO	¹³ CO	N ₂ O	¹² CO,N ₂ O	¹³ CO,N ₂ O		CO	N ₂ O	CO,N ₂ O
¹² C3N1	0.77	0.00	0.15	0.08	0.00	¹² C3N1	0.77	0.15	0.08
¹³ C1 ¹² C2N1	0.58	0.24	0.12	0.04	0.02	¹³ C1 ¹² C2N1	0.82	0.12	0.06
¹³ C2 ¹² C1N1	0.28	0.49	0.14	0.03	0.06	¹³ C2 ¹² C1N1	0.77	0.14	0.09
¹³ C3N1	0.00	0.77	0.15	0.00	0.09	¹³ C3N1	0.77	0.15	0.09
C3N2									
	¹² CO	¹³ CO	N ₂ O	¹² CO,N ₂ O	¹³ CO,N ₂ O		CO	N ₂ O	CO,N ₂ O
¹² C3N2	0.56	0.00	0.33	0.11	0.00	¹² C3N2	0.56	0.33	0.11
¹³ C1 ¹² C2N2	0.30	0.17	0.33	0.13	0.07	¹³ C1 ¹² C2N2	0.47	0.33	0.20
¹³ C2 ¹² C1N2	0.20	0.29	0.33	0.07	0.11	¹³ C2 ¹² C1N2	0.49	0.33	0.18
¹³ C3N2	0.00	0.47	0.36	0.00	0.17	¹³ C3N2	0.47	0.36	0.17

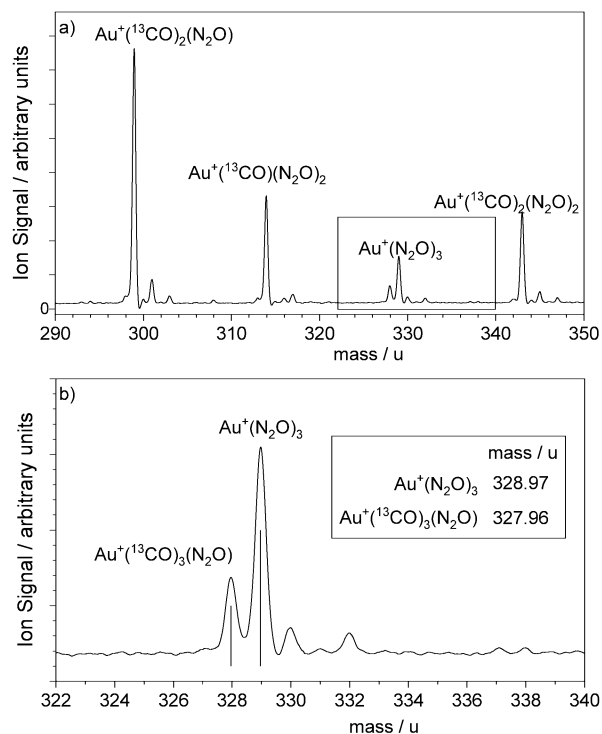


Figure S1: a) Portion of the time-of-flight mass spectrum of $\text{Au}(\text{}^{13}\text{CO})_n(\text{N}_2\text{O})_m^+$ complexes produced by laser ablation of a gold target in presence of a carrier gas comprising 1% ^{13}CO and 5% N_2O in Ar, illustrating clear mass resolution of the peaks of interest. b) The spectrum around $m/z = 330$ u showing internal consistency of the calibration performed to the major peaks observed in the spectrum. *n.b.*, both a) and b) are shown before application of the quadrupole mass filter used for mass selectivity prior to action spectroscopy.

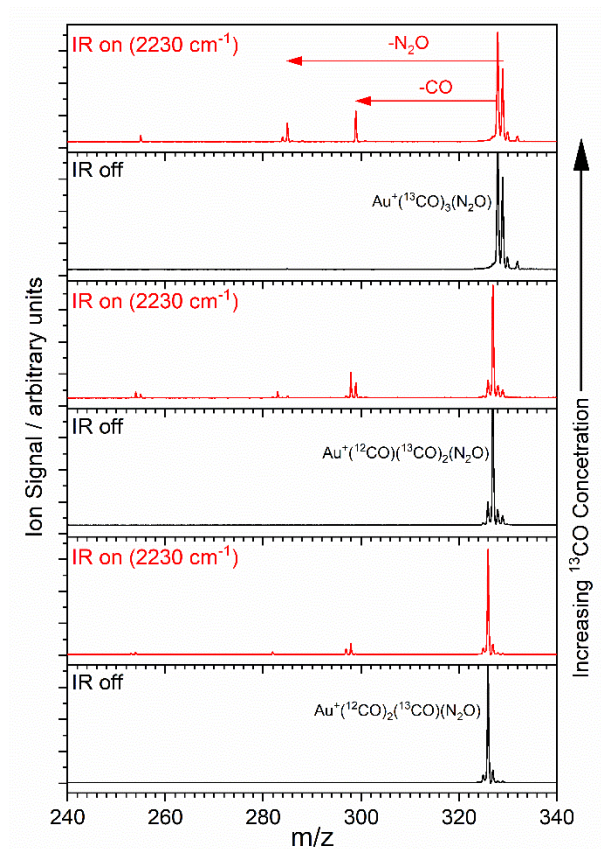


Figure S2: Representative parent ion and 2230 cm^{-1} photofragment mass spectra for different $^{12}\text{CO}:^{13}\text{CO}$ ratios in the region of the $\text{Au}^+(\text{CO})_3(\text{N}_2\text{O}) / \text{Au}^+(\text{N}_2\text{O})_3$ parent cluster ions. *n.b.* the parent ion distribution (black) reflects both the gas mix and quadrupole mass selectivity, which are optimized for the species of interest. The upper panels represent the near 100% ^{13}CO mix whose full mass spectrum (without mass selection) is shown in Figure S1.

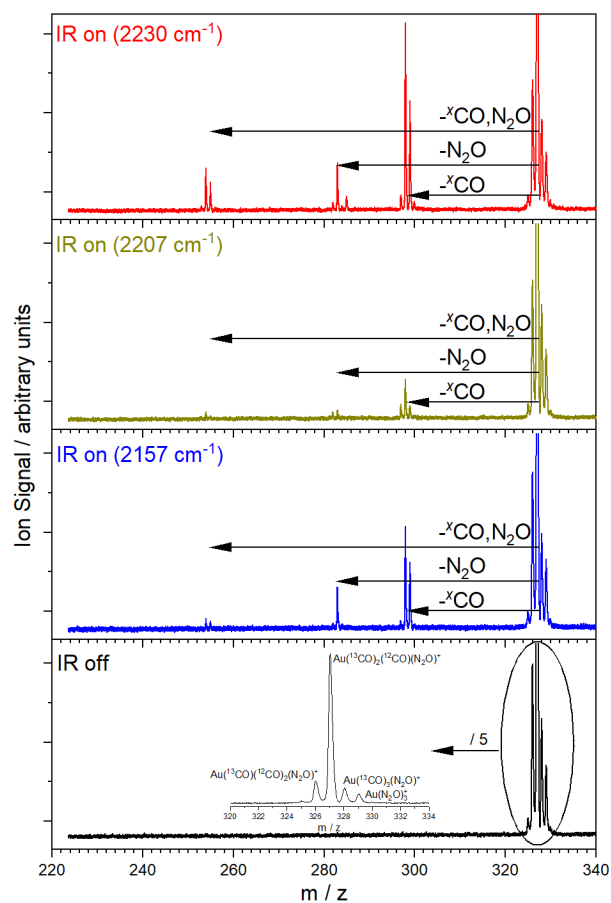


Figure S3: Representative mass spectra of the $\text{Au}({}^{13/12}\text{CO})_3(\text{N}_2\text{O})^+$ with IR off (black) and illustrating mass spectra following photofragmentation at 2157 cm^{-1} (blue), 2207 cm^{-1} (yellow), and 2230 cm^{-1} (red). *n.b.* the parent ion distribution (black) reflects both the gas mix and quadrupole mass selectivity, which are optimized for the species of interest.

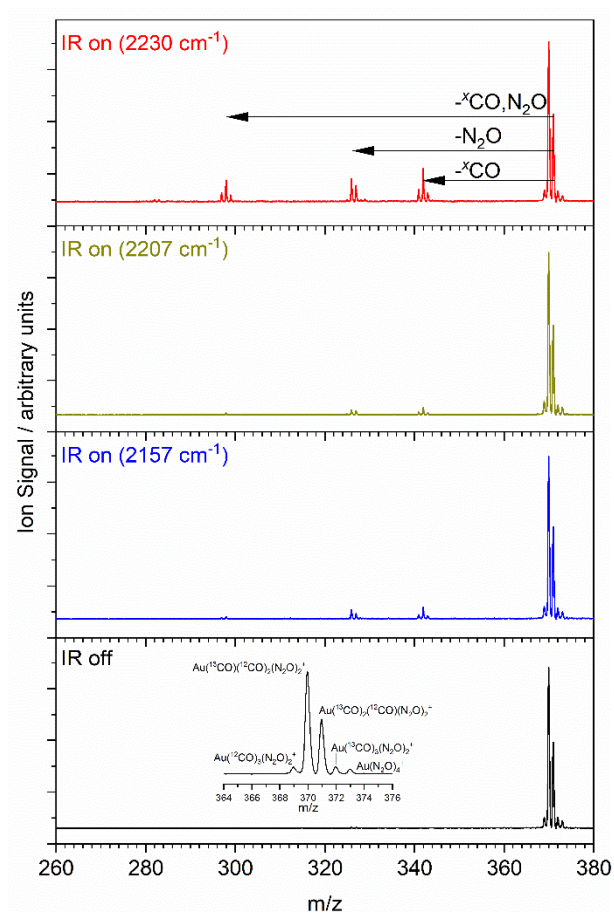


Figure S4: Representative mass spectra of the $\text{Au}^{(13/12)\text{CO}}_3(\text{N}_2\text{O})_2^+$ with IR off (black) and illustrating mass spectra following photofragmentation at 2157 cm^{-1} (blue), 2207 cm^{-1} (yellow), and 2230 cm^{-1} (red). *n.b.* the parent ion distribution (black) reflects both the gas mix and quadrupole mass selectivity, which are optimized for the species of interest.

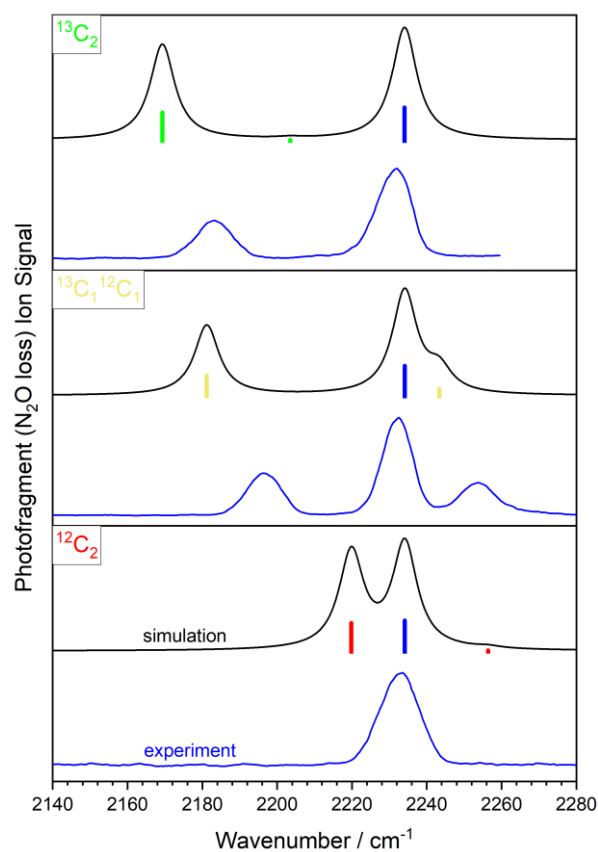


Figure S5: Comparison of experimental and simulated infrared action spectra of $\text{Au}({}^{13/12}\text{CO})_2(\text{N}_2\text{O})^+$ complexes. Modes associated with N_2O are scaled with respect to the $\text{N}=\text{N}$ stretch in free N_2O stretch (2223.5cm^{-1} , $\text{SF} = 0.9322$) and CO modes are scaled to the free CO stretch (2143.2cm^{-1} , $\text{SF} = 0.9626$).

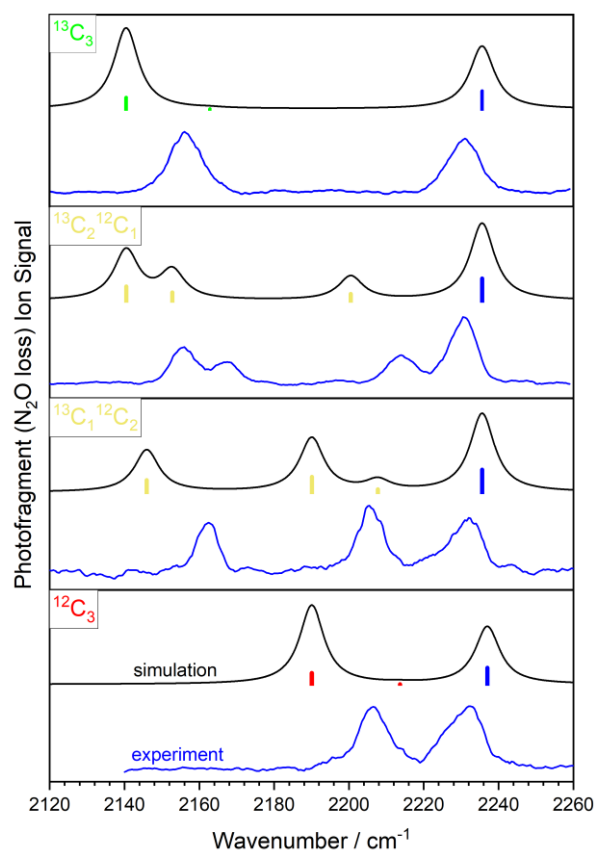


Figure S6: Comparison of experimental and simulated infrared action spectra of $\text{Au}({}^{13/12}\text{CO})_3(\text{N}_2\text{O})^+$ complexes. Modes associated with N_2O are scaled with respect to the $\text{N}=\text{N}$ stretch in free N_2O stretch (2223.5cm^{-1} , $\text{SF} = 0.9322$) and CO modes are scaled to the free CO stretch (2143.2cm^{-1} , $\text{SF} = 0.9626$).

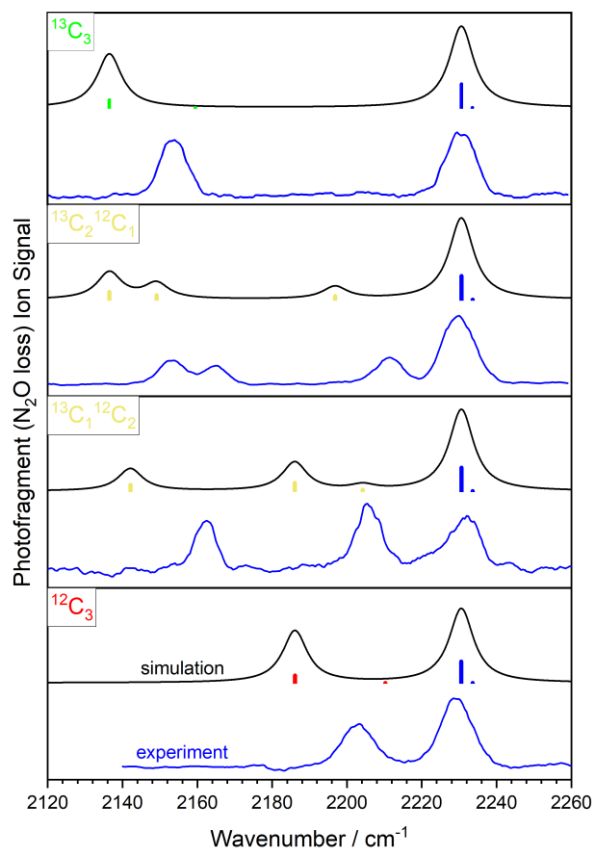


Figure S7: Comparison of experimental and simulated infrared action spectra of $\text{Au}(^{13/12}\text{CO})_3(\text{N}_2\text{O})_2^+$ complexes. Modes associated with N_2O are scaled with respect to the $\text{N}=\text{N}$ stretch in free N_2O stretch (2223.5cm^{-1} , $\text{SF} = 0.9322$) and CO modes are scaled to the free CO stretch (2143.2cm^{-1} , $\text{SF} = 0.9626$).

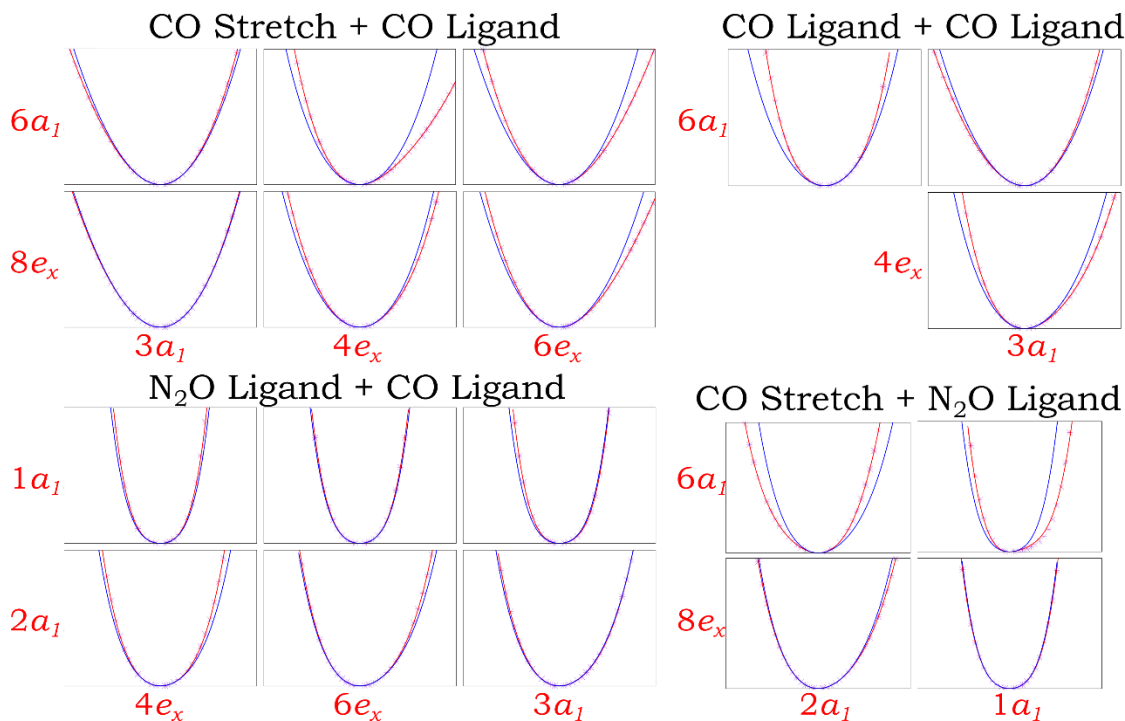


Figure S8: Potential energy surface cuts along the positive quadrant of two modes. These modes belong to pairs of sets of modes that have significant coupling. Correlated and uncorrelated models fitted to the data are also plotted. The purple stars indicate the ab-initio points, the blue line corresponds to the value of the uncorrelated 1-mode fit, whilst the red line to that of the correlated model fit.

The following is an expanded description of the vibrational coupling analysis detailed in the main text. The IR-pumped first vibrational excited state will heat the rest of the system via anharmonic terms in the potential energy surface. Although the system will undergo substantial geometric changes upon dissociation, the early transfer of energy away from $v = 1$ will likely be driven by small anharmonic coupling terms. Table S3 shows the harmonic frequencies for the $^{12}\text{C}^{13}\text{N}$ system. Naturally, the number of degrees of freedom (DOF) involved in CO ligand motion (9) is larger than for N_2O (4). To analyse the coupling between modes, whilst keeping the analysis tractable, we have selected subsets of modes. These naturally describe; the N_2O stretch (2 a_1 modes), N_2O ligand (2 a_1 modes), the CO stretch (1 a_1 and 1 e mode) and the CO Ligand motion of the CO aligned with the x-axis (1 a_1 and 2 e modes). We evaluated hundreds of ab-initio points along each of the linear cuts of all symmetrically unique quadrants of all possible pairs in the aforementioned subset, as well (quasi random) sobol-sampled the same correlated space. We used mass and frequency scaled normal mode coordinates to approximately place all displacements into a similar domain. We then fitted a cluster expansion of symmetry-adapted polynomial functions to the calculated data. For doubly degenerate e modes, we included both degenerate terms; for example, $e \times e$ is a four-dimensional correlated space. Most clusters require between fourth to sixth order polynomials to fit the data with minimal error (average RMSD $< 10^{-5}$ eV). Figure S5 shows PES cuts along the positive quadrant for some of the more significant pairs of correlated coordinates for the domain $(-0.22, 0.22)$ bohr amu^{-1} and range up to 0.5 eV. The purple stars indicate the ab-initio points, the blue line corresponds to the value of the uncorrelated 1-mode fit, whilst the red line to that of the correlated model fit. The discrepancy between the two lines gives a *qualitative* assessment of the degree of correlation between the modes; we found that

the extent of the discrepancy along this quadrant is reasonably representative of the entire correlated space. To better quantify the extent of correlation between these modes, we calculated the Boltzmann-sampled root mean squared deviation (RMSD) between the correlated and uncorrelated models. This is done for each possible pair of modes. We used a sampling temperature of 150 K. Table 1 (in the main text) shows the average RMSD values of the mode-pairs, for each possible pair of subsets. This provides us with a more quantitative measure of the extent of coupling between the differing types of motion.